IET Power Electronics

Special Issue: Advanced Technologies Utilised in Wireless Power Transfer Systems

IET Journals
The Institution of Engineering and Technology

Underwater wireless power transfer system with a curly coil structure for AUVs

ISSN 1755-4535
Received on 14th October 2018
Revised 31st January 2019
Accepted on 15th February 2019
E-First on 8th March 2019
doi: 10.1049/iet-pel.2018.6090
www.ietdl.org

Zhengchao Yan[1,2], Yiming Zhang[2], Kehan Zhang[1], Baowei Song[1], Chris Mi[2] ✉

[1]*School of Marine Science and Technology, Northwestern Polytechnical University, 127 West Youyi Road, Xi'an, People's Republic of China*
[2]*Department of Electrical and Computer Engineering, San Diego State University, 5500 Campanile Drive, San Diego, CA, USA*
✉ *E-mail: mi@ieee.org*

Abstract: An underwater wireless power transfer system with a curly coil structure is proposed to adapt to the cylindrical symmetric hull of the autonomous underwater vehicles (AUVs). The unipolar and bipolar curly coils are optimised to minimise the weight of the receiver with the same output power. It is revealed that the bipolar curly coil structure has a heavier receiver than the unipolar curly coil structure. However, the electromagnetic field radiation in the AUV of the bipolar curly coil structure is much smaller than that of the unipolar curly coil structure, which means that the bipolar curly coil structure has a smaller influence on the electronics components in the AUV. Therefore, the bipolar curly coil is adopted for the prototype. The series−series (SS) and double-sided inductor−capacitor−capacitor (LCC−LCC) compensation topologies for the bipolar curly coil structure are also investigated. A prototype was built and the experimental results showed that distorted coil currents are generated in the SS compensation topology, while the LCC−LCC compensation has a nearly sinusoidal coil current. The efficiencies of the SS and LCC−LCC compensation topologies are approximately the same, at ∼95%, which indicates that the proposed curly coil structure is applicable.

1 Introduction

Wireless power transfer (WPT) is widely used in diverse scenarios [1–4], such as electric vehicles (EVs), electric bicycles, and autonomous underwater vehicles (AUVs). The research focus covers the power electronics converters, compensation topologies [5], coil optimisation [6], foreign object detection [7], and safety issues [8]. Among these fields, the coil optimisation is crucial to increase the overall efficiency and minimise the size, weight, and cost of the WPT system, especially for the receiver side with a restricted requirement.

In the fields of the coil optimisation, the different coil structures have been extensively investigated. A loosely coupled unipolar coil was designed to minimise the electromagnetic field (EMF) radiation in the concerned areas [9]. Budhia *et al.* [10] designed and optimised the circular unipolar coils and built a 2 kW 700-mm diameter pad. A 3-D omnidirectional coil, which was composed of three unipolar coils and driven by a rotating current vector, was investigated. It showed that the direction of the maximum input power vector was the same as that of the maximum energy efficiency, which provided a useful tool to detect the load location [11]. Besides the unipolar coil structures, the bipolar coil structure has also been widely adopted in WPT systems for its high efficiency and misalignment tolerance. The magnetic analysis of the bipolar coil was conducted in a distributed WPT system, in which the magnetic field was longitudinal to the coil plane [12]. In the inductor−capacitor−capacitor-compensated WPT systems, the compensation inductors can be integrated with the main coils, achieving a compact magnetic coupler. A method that integrated the bipolar compensation coil into the unipolar main coil was proposed, realising a compact system size and eliminating the extra coupling [13]. A WPT system based on a relay resonator was investigated, which showed that the relay-based WPT systems had a larger transfer efficiency compared to that of the two-coil-based systems [14].

The coil structures mentioned above are difficult to perfectly adapt to the cylindrical hull of the AUV. In order to improve the hydrodynamic performance of the AUV, a hull-compatible coaxial coil structure was developed and the efficiency was optimised by evaluating the power losses of different parts [15]. However, the magnetic field is divergent to the centre of the coil, which would affect the electronics components in the AUV. In order to solve this problem, a three-phase WPT system was proposed and the solenoid coil structure was used, which can be compatible with the AUV's hull and has concentrated magnetic field. The system can achieve 1 kW under a 92.41% DC−DC efficiency. However, the system efficiency and output power will decrease dramatically with the rotational misalignment [16]. Therefore, another three-phase WPT system was proposed which not only preserved the merits of the former one, but also improved the performance during the rotational misalignments [17]. However, this coil structure needs modification to the AUV's hull, and the size of the receiver is large due to the three toroidal coils need for the design which might limit the application of the proposed technology.

This paper proposes an underwater WPT system with a hull-compatible curly coil structure to charge the AUV. The curly coil structure facilitates the installation of the WPT system to the hull of the AUV without additional alteration, and it is easy to shield the magnetic field. The unipolar and bipolar curly coils are designed and optimised by a finite element analysis tool. The series−series (SS) and double-sided inductor−capacitor−capacitor (LCC−LCC) compensation topologies for the curly coil structure are also analysed. A WPT prototype is set up to validate the analysis.

2 Coil design

The proposed curly coil structure is shown in Fig. 1. The curly coil is hull-compatible and can be embedded in the AUV's hull, which can spare a lot of space for the AUV. The ferrite is used at the back of the coil to improve the coupling between the transmitter and the receiver and decrease the electromagnetic radiation. Due to the outer diameter of the AUV, the radius of the receiver coil R_2 is set to 150 mm, and the gap between the transmitter and the receiver is fixed at 10 mm.

Due to the hull-compatible curly coil structure, the receiver can be embedded into the AUV's hull. Therefore, the receiver size is no longer a restriction on the AUV. However, the weight is still a concern on the AUV due to the long voyage target, and the EMF radiation in the AUV is another issue which should be considered to protect the electronics components.

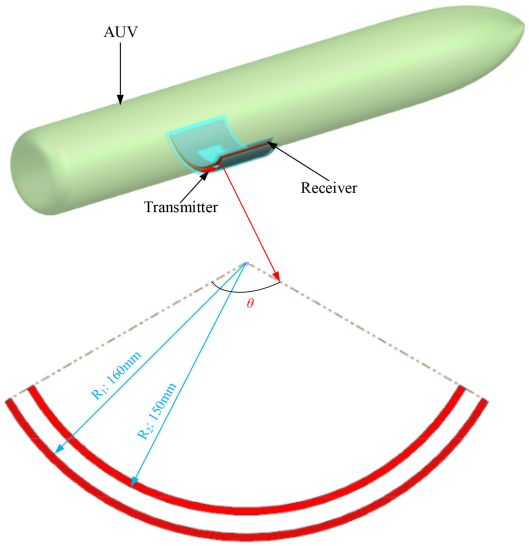

Fig. 1 *Proposed curly coil structure*

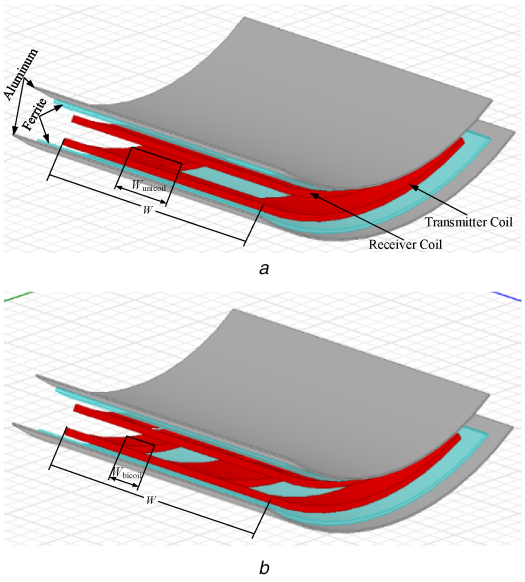

Fig. 2 *Coil structures*
(a) Unipolar,
(b) Bipolar

2.1 Weight calculation

The transmitter is installed in the stationary base station with no weight restrictions. Therefore, we only optimise the weight of the receiver in this paper. The output power of two inductively coupled coils is maximised when the phase difference between the transmitter and receiver currents is 90° [18], which can be expressed as

$$P_{\text{out}} = \omega_0 M I_1 I_2 = \omega_0 k \sqrt{L_{10} L_{20}} N_1 I_1 N_2 I_2 \tag{1}$$

where ω_0 is the resonant angular frequency, I_1 (I_2) is the transmitter (receiver) current, L_{10} (L_{20}) is the single-turn self-inductance of the transmitter (receiver), N_1 (N_2) is the turn number of the transmitter (receiver), M and k are the mutual inductance and the coupling coefficient between the transmitter and the receiver, respectively.

In this paper, the output power is 1000 W. The unipolar and bipolar coils, which are shown in Fig. 2, are optimised for the AUV. The outer width of the coil W is set to 160 mm, the ferrite is 20 mm wider than the coil, the aluminium is 20 mm wider than the ferrite, and the open angle θ varies from 50° to 120°. Then k, L_{10}, and L_{20} can be obtained via the finite element analysis tool ANSYS Maxwell. In the simulations, the type of the ferrite is 3C95, the saturation magnetic flux density is 0.5 T, and the relative

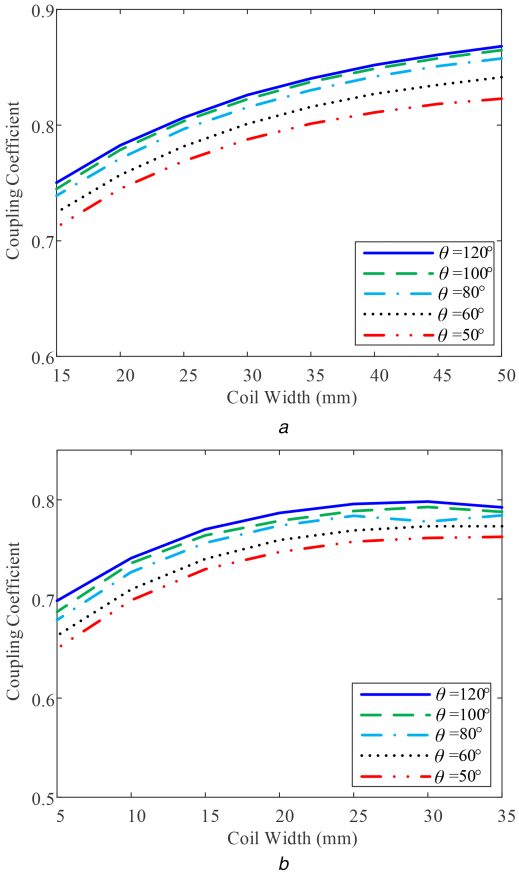

Fig. 3 *Coupling coefficient varying with the coil width*
(a) Unipolar,
(b) Bipolar

permeability is 3300. The coupling coefficient varying with the coil width under different open angles is shown in Fig. 3. The coupling coefficient increases with an increasing coil width and then reaches a relatively stable value, which is seen as saturation. So in the increasing range, we can increase the coil width to increase the coupling coefficient until it is saturated. It can be seen from Fig. 3*a* that the coupling coefficient of the unipolar curly coil is saturated when the coil width is 40 mm under different open angles. Fig. 3*b* shows that the coupling coefficient of the bipolar curly coil is saturated when the coil width is 20 mm.

We fixed the coil width of the unipolar and bipolar curly coils at 40 and 20 mm, respectively, and assume that the ampere-turn of the transmitter equals that of the receiver, namely, $N_1 I_1 = N_2 I_2 = NI$. The targeted P_{out} is 1000 W. Then the ampere-turn can be calculated as

$$NI = \sqrt{\frac{P_{\text{out}}}{\omega_0 k \sqrt{L_{10} L_{20}}}} \tag{2}$$

By substituting the ampere-turn into the current excitation of the ANSYS Maxwell, the maximum magnetic flux density B_{max} in the ferrite can be obtained. The design requirement is $B_{\text{max}} \leq 0.2$ T, because 0.2 T is in the linear segment of the BH curve of the 3C95 ferrite and close to the inflection point of the BH curve. Also, the power loss is smaller at a smaller magnetic flux density under the same temperature and frequency. Table 1 shows the maximum magnetic flux density in the ferrite. It can be seen that the magnetic flux density in the ferrite of the unipolar coil structure is smaller than that in the ferrite of the bipolar coil structure, which is because the smaller ampere-turns of the unipolar coil structure.

The weight of the copper for the unipolar curly coil $m_{\text{copper\_uni}}$ can be calculated as

$$m_{\text{copper\_uni}} = \left(2\left(2\pi R_2 \frac{\theta}{360^\circ} - W_{\text{unicoil}}\right) + 2(W - W_{\text{unicoil}})\right)\frac{NI}{J}\rho_{\text{copper}} \quad (3)$$

where W_{unicoil} is the coil width of the unipolar curly coil, ρ_{copper} is the density of the copper, and J is the current density, which is set to 4 A/mm^2.

The corresponding copper weight of the bipolar curly coil $m_{\text{copper\_bi}}$ is

$$m_{\text{copper\_bi}} = \left(4\left(2\pi R_2 \frac{\theta}{360^\circ} - W_{\text{bicoil}}\right) + 2(W - 2W_{\text{bicoil}})\right)\frac{NI}{J}\rho_{\text{copper}} \quad (4)$$

where W_{bicoil} is the coil width of the bipolar curly coil. With the same calculation method, the ferrite weight and the aluminium weight of the unipolar and bipolar curly coil, namely $m_{\text{ferrite\_uni}}$, $m_{\text{ferrite\_bi}}$, $m_{\text{aluminum\_uni}}$, and $m_{\text{aluminum\_bi}}$, can be obtained. Then the total weight of the receiver can be obtained as

$$\begin{cases} m_{\text{total\_uni}} = m_{\text{copper\_uni}} + m_{\text{ferrite\_uni}} + m_{\text{aluminum\_uni}} \\ m_{\text{total\_bi}} = m_{\text{copper\_bi}} + m_{\text{ferrite\_bi}} + m_{\text{aluminum\_bi}} \end{cases} \quad (5)$$

Table 2 shows the total weight of the receiver for the unipolar and bipolar curly coil structure. To meet the requirement of the maximum magnetic flux density and the minimum receiver weight, it can be seen from Tables 1 and 2 that the open angle θ of the unipolar and bipolar curly coil should both equal 60°. The receiver ferrite thickness of the unipolar curly coil equals 1 mm and the receiver ferrite thickness of the bipolar curly coil equals 2 mm. The receiver weight of the bipolar coil is 521.1 g, which is heavier than that of the unipolar coil weight of 363.4 g.

2.2 EMF radiation

The system parameters are settled by the above procedure. Then the EMF radiation in the AUV should be considered. Fig. 4 shows the magnetic field distribution of the unipolar and bipolar curly coil structures in the cross-section under the same output power and operating frequency with the optimised receiver weight point. It can be seen that the bipolar curly coil structure has a less EMF radiation compared to the unipolar curly coil structure, which means that the electronics components in the AUV can be well protected by using the bipolar curly coil structure. When we increase the receiver ferrite thickness of the unipolar curly coil structure to 2 mm, which is the same as that of the bipolar curly coil structure, we can see in Fig. 5 that the bipolar curly coil structure has a smaller EMF radiation. The flow diagram of the system design procedure is shown in Fig. 6.

Above all, the unipolar and bipolar curly coil structures both have merits and demerits. Based on the priorities of different practical applications, the specific curly coil structure (unipolar or bipolar) can be determined. In this paper, we target a small AUV and since the size is small, which means that the EMF radiation will affect more inside the AUV. Although the receiver weight of the bipolar coil is 521.1 g, which is more than that of the unipolar coil of 363.4 g, the receiver weight of both the bipolar and unipolar coil structures can be accepted by the AUV's loading capacity. Therefore, we choose the bipolar coil for the AUV to better protect the electronics components in the AUV. If the required power is lager, the receiver weight will be larger too due to the larger required dimension of the receiver, and then the receiver weight may become the priority of the system design.

3 Topology comparison

The SS and LCC−LCC compensation topologies are widely used in WPT systems due to their symmetric parameters and constant-current output characteristic. Therefore, the comparison is made between these two topologies.

Table 1 Maximum magnetic flux density in the ferrite

θ°	Unipolar				Bipolar			
	h, mm							
	0.5	1	1.5	2	0.5	1	1.5	2
50	0.32	0.21	0.14	0.08	0.60	0.33	0.22	0.21
60	0.30	0.20	0.12	0.08	0.52	0.33	0.25	0.20
70	0.35	0.17	0.12	0.08	0.58	0.30	0.25	0.18
80	0.30	0.17	0.13	0.12	0.64	0.30	0.20	0.18
90	0.33	0.20	0.13	0.12	0.61	0.4	0.19	0.16
100	0.39	0.16	0.11	0.09	0.51	0.34	0.17	0.16
110	0.29	0.19	0.11	0.08	0.48	0.24	0.17	0.15
120	0.29	0.22	0.11	0.08	0.43	0.31	0.16	0.14

Note: *h* denotes the ferrite thickness of the receiver. The unit for the maximum flux density is T.

Table 2 Total weight of the receiver

θ°	Unipolar				Bipolar			
	h, mm							
	0.5	1	1.5	2	0.5	1	1.5	2
50	260.6	322.6	384.3	445.8	270.7	332.4	394.2	455.1
60	291.0	363.4	435.9	508.3	304.0	376.1	448.8	521.1
70	322.2	405.7	489.0	572.1	336.8	420.1	503.4	586.5
80	353.6	448.1	542.3	636.3	369.6	463.9	557.7	652.0
90	385.8	491.2	596.1	701.1	402.9	508.0	613.1	717.8
100	418.1	534.2	650.0	765.8	436.2	552.3	668.1	783.9
110	450.4	577.1	703.8	830.2	469.5	595.7	722.4	848.5
120	482.6	620.2	757.8	895.1	502.5	639.9	777.5	914.5

The unit for the total weight of the receiver is g.

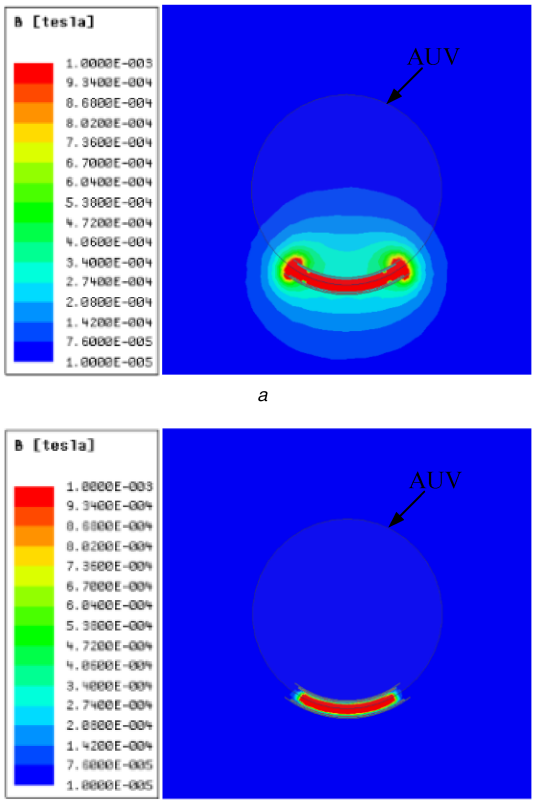

Fig. 4 *Magnetic field distribution in the cross-section*
(a) Unipolar: open angle is 60° and receiver ferrite thickness is 1 mm,
(b) Bipolar: open angle is 60° and receiver ferrite thickness is 2 mm

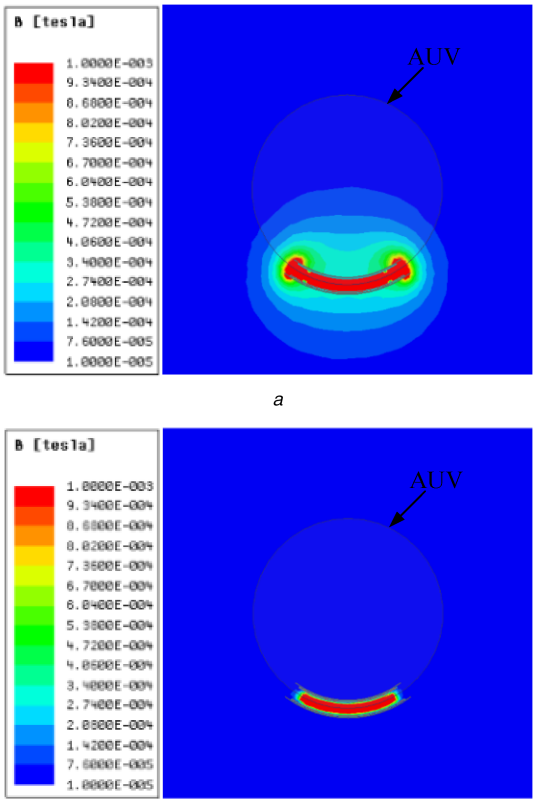

Fig. 5 *Magnetic field distribution in the cross-section*
(a) Unipolar: open angle is 60° and receiver ferrite thickness is 2 mm,
(b) Bipolar: open angle is 60° and receiver ferrite thickness is 2 mm

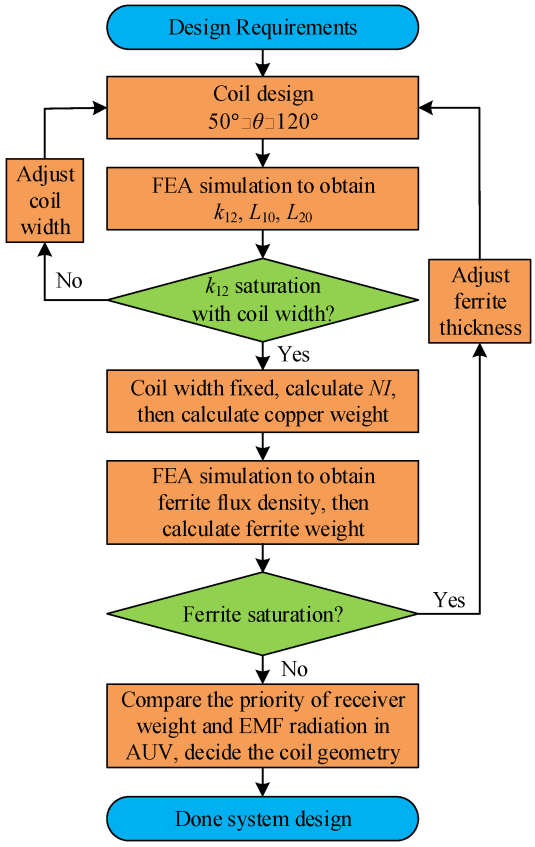

Fig. 6 *Flow diagram of the system design procedure*

3.1 SS topology

The circuit topology of the proposed WPT system with SS topology is depicted in Fig. 7*a*. L_1 (L_2) is the transmitter (receiver) inductance, C_1 (C_2) is the series compensation capacitance, U_{bus} (U_{bat}) is the inverter (battery) DC voltage, U_1 (U_2) is the inverter (rectifier) AC voltage, I_1 (I_2) is the transmitter (receiver) current, and M_{12} is the mutual inductance between L_1 and L_2.

The receiver current at resonance is

$$I_2 = \frac{U_1}{\omega_0 M} \tag{6}$$

The SS topology has a constant-current output. The output power can be expressed as

$$P_{\text{out\_SS}} = U_2 I_2 = \frac{8 U_{\text{bus}} U_{\text{bat}}}{\pi^2 \omega_0 k N_{\text{SS}}^2 \sqrt{L_{10} L_{20}}} \tag{7}$$

We fix $U_{\text{bus}} = U_{\text{bat}} = 130$ V and $P_{\text{out\_SS}} = 1000$ W, and the turn number N_{SS} can be calculated as

$$N_{\text{SS}} = \frac{\pi}{2\sqrt{2}} \sqrt{\frac{U_{\text{bus}} U_{\text{bat}}}{\omega_0 k P_{\text{out}} \sqrt{L_{10} L_{20}}}} = 5.8 \tag{8}$$

Therefore, the turn number is set to 6.

3.2 LCC-−LCC topology

The LCC–LCC topology of the proposed WPT system is depicted in Fig. 7*b*. L_{f3} (L_{f4}) is the compensation inductance, C_3 (C_4) is the series compensation capacitance, C_{f3} (C_{f4}) is the parallel compensation capacitance, U_{bus} (U_{bat}) is the inverter (battery) DC voltage, U_3 (U_4) is the inverter (rectifier) AC voltage, I_{f3} (I_{f4}) is the inverter (rectifier) ac current, and I_3 (I_4) is the transmitter (receiver) current.

The rectifier AC current at resonance is

$$I_{f4} = \frac{MU_3}{\omega_0 L_{f3} L_{f4}} \tag{9}$$

The LCC−LCC topology also has a constant-current output. The output power at resonance is

$$P_{\text{out\_LCC}} = U_4 I_{f4} = \frac{8kU_{\text{bus}}U_{\text{bat}}}{\pi^2 \omega_0 \alpha^2 N_{\text{LCC}}^2 \sqrt{L_{10}L_{20}}} \tag{10}$$

where α denotes the ratio of the compensation inductance and the main inductance. We also fix $U_{\text{bus}} = U_{\text{bat}} = 130$ V and $P_{\text{out\_LCC}} = 1000$ W, then the turn number N_{LCC} can be calculated as

$$N_{\text{LCC}} = \sqrt{\frac{kU_3U_4}{\omega_0 \alpha^2 P_{\text{out}} \sqrt{L_{10}L_{20}}}} = \frac{\pi}{2\sqrt{2}} \sqrt{\frac{kU_{\text{bus}}U_{\text{bat}}}{\omega_0 \alpha^2 P_{\text{out}} \sqrt{L_{10}L_{20}}}} \tag{11}$$

Assuming $\alpha = k$, N_{LCC} also equals 5.8. Therefore, the turn number is also set to 6.

4 Calculations and experiments

A prototype based on the proposed bipolar curly coil is implemented, as shown in Fig. 8. The system specifications and the circuit parameters are listed in Table 3. The width of the coil is 160 mm and the open angle is 60°, and the turn numbers of the transmitter and the receiver are both 6. Since the transmitter and the receiver are coaxial and have the same open angle, the transmitter is a little larger than the receiver, resulting in a larger self-inductance.

Fig. 9 shows the voltage and current waveforms of the SS and LCC−LCC compensation topologies. U_{bus} and U_{bat} are both 130 V. It can be seen that the coil currents of the SS topology are distorted, while the currents of the LCC−LCC topology remain relatively sinusoidal due to the different input impedances of different topologies caused by the large coupling coefficient.

U_{bus} is fixed at 130 V, and U_{bat} changes from 50 to 130 V. Fig. 10 shows the output power and DC−DC efficiency of the SS and LCC−LCC topology varying with the input DC voltage. It can be noted from Fig. 10*a* that the output power of the SS topology is nearly identical to that of the LCC−LCC topology, which verifies the analysis in Section 3. Fig. 10*b* indicates that the DC−DC efficiency of the SS topology is roughly 1% higher than that of the LCC−LCC topology, even though the coil currents are distorted. This is because there are six compensation components in the LCC −LCC topology, which results in extra loss in the system compare to the SS topology. However, both topologies can be selected in the practical applications for their high efficiencies and constant-current output.

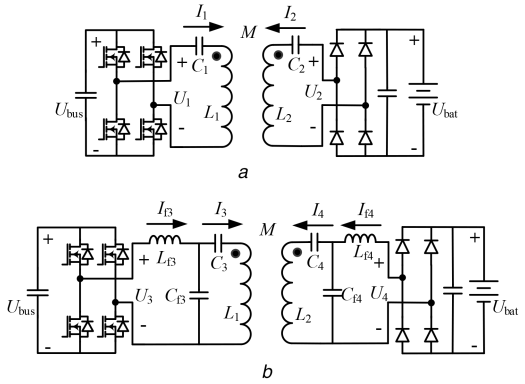

Fig. 7 *Different topologies*
(a) SS,
(b) LCC−LCC

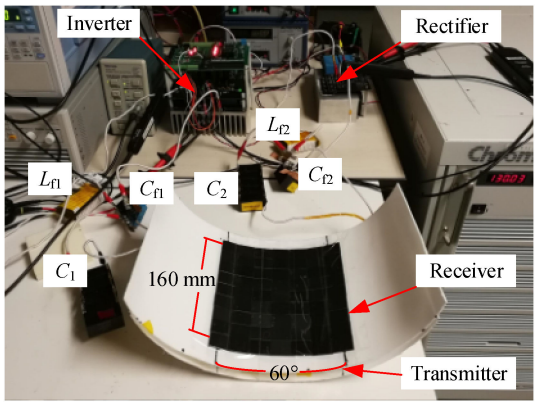

Fig. 8 *Experimental prototype*

Table 3 System specifications and circuit parameters

U_{bus}	U_{bat}	L_{f3}	L_{f2}	L_1	L_2
130 V	130 V	25.7 μH	25.5 μH	32.8 μH	32.6 μH
k	C_{f3}	C_{f4}	C_3	C_4	f_{LCC}
0.784	138.3 nF	140.4 nF	498.9 nF	504 nF	84.3 kHz
C_1	C_2	f_{SS}	θ	W	Gap
106.9 nF	107.5 nF	85 kHz	60°	160 mm	10 mm

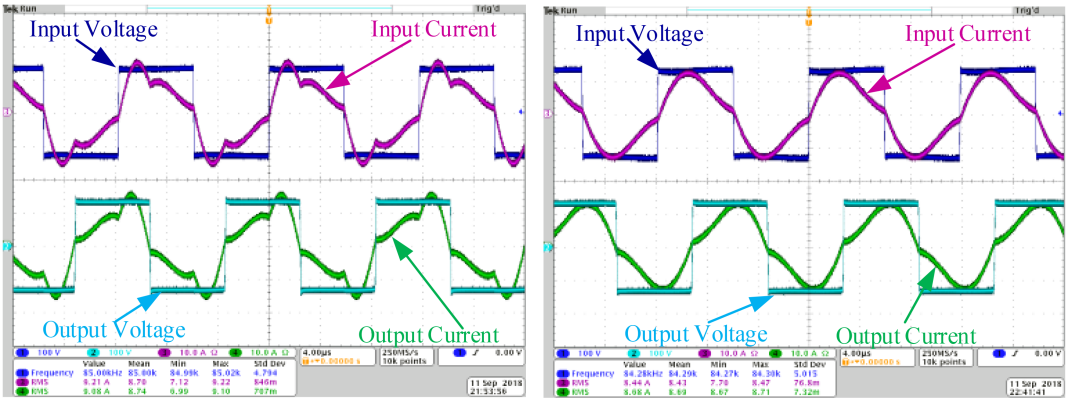

a *b*

Fig. 9 *Voltage and current waveforms when P_{out} = 1000 W*
(a) SS,
(b) LCC−LCC

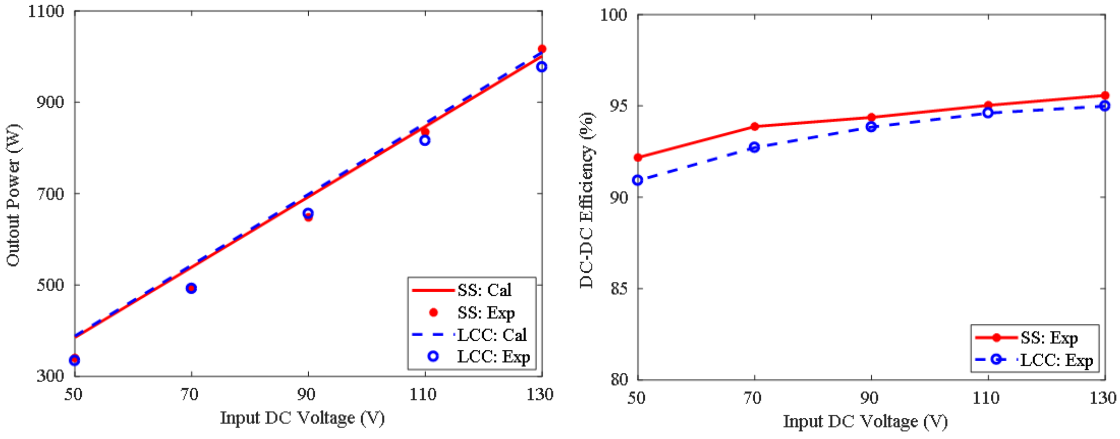

a *b*

Fig. 10 *Output power and DC−DC efficiency versus the input voltage*
(a) Output power,
(b) DC−DC efficiency

5 Conclusion

An underwater WPT system with a curly coil structure has been proposed to charge the AUV. The receiver can be adapted to the cylindrical symmetric hull of the AUV. The unipolar and bipolar curly coils have been optimised. It has been found that the optimised open angles of both coil structures are 60° and the receiver weight of the bipolar curly coil structure is heavier than that of the unipolar curly coil structure. However, the EMF radiation in the AUV of the bipolar curly coil structure is much smaller than that of the unipolar curly coil structure, which means that the bipolar curly coil structure has a smaller influence on the electronics components in the AUV. A 1000 W prototype has been built and the experimental results showed that the coil currents of the SS topology are distorted, while the currents of the LCC−LCC topology remain relatively sinusoidal. The DC−DC efficiency of the SS topology is nearly the same as that of the LCC topology, both at ∼95%, which indicates that the proposed curly coil structure is applicable.

6 Acknowledgments

This work was supported by the Natural Science Basic Research Plan in Shaanxi Province of China (Grant No. 2018JM5033) and the China Scholarship Council (Grant No. 201706290074).

7 References

[1] Zhang, Y., Kan, T., Yan, Z., *et al.*: 'Modeling and analysis of series-none compensation for wireless power transfer systems with a strong coupling', *IEEE Trans. Power Electron.*, 2019, **34**, (2), pp. 1209–1215

[2] Beh, H.Z., Covic, G.A., Boys, J.T.: 'Wireless fleet charging system for electric bicycles', *IEEE J. Emerging Sel. Topics Power Electron.*, 2015, **3**, (1), pp. 75–86

[3] Mai, R.K., Chen, Y., Li, Y., *et al.*: 'Inductive power transfer for massive electric bicycles charging based on hybrid topology switching with a single inverter', *IEEE Trans. Power Electron.*, 2017, **32**, (8), pp. 5897–5906

[4] Yan, Z., Zhang, Y., Kan, T., *et al.*: 'Frequency optimization of a loosely coupled underwater wireless power transfer system considering eddy current loss', *IEEE Trans. Ind. Electron.*, 2019, **66**, (5), pp. 3468–3476

[5] Villa, J.L., Sallan, J., Osorio, J.F.S., *et al.*: 'High-misalignment tolerant compensation topology for ICPT systems', *IEEE Trans. Ind. Electron.*, 2012, **59**, (2), pp. 945–951

[6] Kim, S., Covic, G.A., Boys, J.T.: 'Comparison of tripolar and circular pads for IPT charging systems', *IEEE Trans. Power Electron.*, 2018, **33**, (7), pp. 6093–6103

[7] Jeong, S.Y., Kwak, H.G., Jang, G.C., *et al.*: 'Dual-purpose non-overlapping coil sets as metal object and vehicle position detections for wireless stationary EV chargers', *IEEE Trans. Power Electron.*, 2018, **33**, (9), pp. 7387–7397

[8] Zhang, K.H., Du, L.N., Zhu, Z.B., *et al.*: 'A normalization method of delimiting the electromagnetic hazard region of a wireless power transfer system', *IEEE Trans. Electromagn. Compat.*, 2018, **60**, (4), pp. 829–839

[9] Zhang, W., White, J.C., Malhan, R.K., *et al.*: 'Loosely coupled transformer coil design to minimize EMF radiation in concerned areas', *IEEE Trans. Veh. Technol.*, 2016, **65**, (6), pp. 4779–4789

[10] Budhia, M., Covic, G.A., Boys, J.T.: 'Design and optimization of circular magnetic structures for lumped inductive power transfer systems', *IEEE Trans. Power Electron.*, 2011, **26**, (11), pp. 3096–3108

[11] Lin, D.Y., Zhang, C., Hui, S.Y.R.: 'Mathematic analysis of omnidirectional wireless power transfer − part-II. Three-dimensional systems', *IEEE Trans. Power Electron.*, 2017, **32**, (1), pp. 613–624

[12] Zaheer, A., Covic, G.A., Kacprzak, D.: 'A bipolar pad in a 10-kHz 300-W distributed IPT system for AGV applications', *IEEE Trans. Ind. Electron.*, 2014, **61**, (7), pp. 3288–3301

[13] Kan, T.Z., Lu, F., Nguyen, T.D., *et al.*: 'Integrated coil design for EV wireless charging systems using LCC compensation topology', *IEEE Trans. Power Electron.*, 2018, **33**, (11), pp. 9231–9241

[14] Lee, J., Lee, K., Cho, D.H.: 'Stability improvement of transmission efficiency based on a relay resonator in a wireless power transfer system', *IEEE Trans. Power Electron.*, 2017, **32**, (5), pp. 3297–3300

[15] Shi, J.G., Li, D.J., Yang, C.J.: 'Design and analysis of an underwater inductive coupling power transfer system for autonomous underwater vehicle docking applications', *J. Zhejiang Univ.-Sci. C-Comput. Electron.*, 2014, **15**, (1), pp. 51–62

[16] Kan, T.Z., Mai, R.K., Mercier, P.P*., et al.*: 'Design and analysis of a three-phase wireless charging system for lightweight autonomous underwater vehicles', *IEEE Trans. Power Electron.*, 2018, **33**, (8), pp. 6622–6632

[17] Kan, T.Z., Zhang, Y.M., Yan, Z.C*., et al.*: 'A rotation-resilient wireless charging system for lightweight autonomous underwater vehicles', *IEEE Trans. Veh. Technol.*, 2018, **67**, (8), pp. 6935–6942

[18] Li, S.Q., Mi, C.C.: 'Wireless power transfer for electric vehicle applications', *IEEE J. Emerging Sel. Topics Power Electron.*, 2015, **3**, (1), pp. 4–17